A LETTERS JOURNAL EXPLORING THE FRONTIERS OF PHYSICS

OFFPRINT

Creep dynamics of viscoelastic interfaces

E. A. JAGLA

EPL, **105** (2014) 46003

Please visit the new website
www.epljournal.org

epl

A Letters Journal Exploring the Frontiers of Physics

AN INVITATION TO SUBMIT YOUR WORK

www.epljournal.org

The Editorial Board invites you to submit your letters to EPL

EPL is a leading international journal publishing original, high-quality Letters in all areas of physics, ranging from condensed matter topics and interdisciplinary research to astrophysics, geophysics, plasma and fusion sciences, including those with application potential.

The high profile of the journal combined with the excellent scientific quality of the articles continue to ensure EPL is an essential resource for its worldwide audience. EPL offers authors global visibility and a great opportunity to share their work with others across the whole of the physics community.

Run by active scientists, for scientists

EPL is reviewed by scientists for scientists, to serve and support the international scientific community. The Editorial Board is a team of active research scientists with an expert understanding of the needs of both authors and researchers.

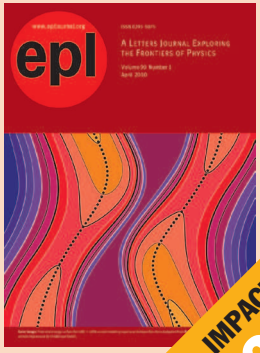

IMPACT FACTOR 2.753*

*As ranked by ISI 2010

IMPACT FACTOR
2.753*
* As listed in the ISI® 2010 Science Citation Index Journal Citation Reports

OVER
500 000
full text downloads in 2010

30 DAYS
average receipt to online publication in 2010

16 961
citations in 2010
37% increase from 2007

"We've had a very positive experience with EPL, and not only on this occasion. The fact that one can identify an appropriate editor, and the editor is an active scientist in the field, makes a huge difference."

Dr. Ivar Martinv
Los Alamos National Laboratory, USA

Six good reasons to publish with EPL

We want to work with you to help gain recognition for your high-quality work through worldwide visibility and high citations.

1. **Quality** – The 40+ Co-Editors, who are experts in their fields, oversee the entire peer-review process, from selection of the referees to making all final acceptance decisions
2. **Impact Factor** – The 2010 Impact Factor is 2.753; your work will be in the right place to be cited by your peers
3. **Speed of processing** – We aim to provide you with a quick and efficient service; the median time from acceptance to online publication is 30 days
4. **High visibility** – All articles are free to read for 30 days from online publication date
5. **International reach** – Over 2,000 institutions have access to EPL, enabling your work to be read by your peers in 100 countries
6. **Open Access** – Articles are offered open access for a one-off author payment

Details on preparing, submitting and tracking the progress of your manuscript from submission to acceptance are available on the EPL submission website **www.epletters.net**.

If you would like further information about our author service or EPL in general, please visit **www.epljournal.org** or e-mail us at **info@epljournal.org**.

EPL is published in partnership with:

European Physical Society | Società Italiana di Fisica | EDP Sciences | IOP Publishing

epl

A Letters Journal
Exploring the Frontiers
of Physics

EPL Compilation Index

www.epljournal.org

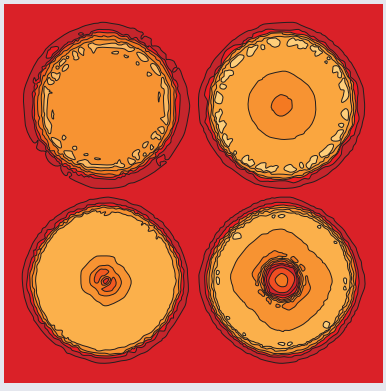

Biaxial strain on lens-shaped quantum rings of different inner radii, adapted from **Zhang *et al*** 2008 EPL **83** 67004.

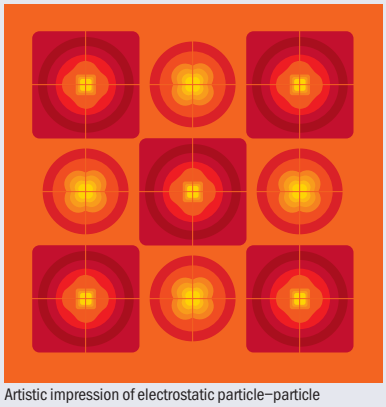

Artistic impression of electrostatic particle–particle interactions in dielectrophoresis, adapted from **N Aubry and P Singh** 2006 *EPL* **74** 623.

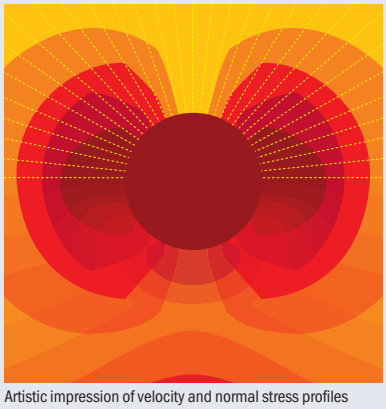

Artistic impression of velocity and normal stress profiles around a sphere that moves through a polymer solution, adapted from **R Tuinier, J K G Dhont and T-H Fan** 2006 *EPL* **75** 929.

Visit the EPL website to read the latest articles published in cutting-edge fields of research from across the whole of physics.

Each compilation is led by its own Co-Editor, who is a leading scientist in that field, and who is responsible for overseeing the review process, selecting referees and making publication decisions for every manuscript.

- Graphene
- Liquid Crystals
- High Transition Temperature Superconductors
- Quantum Information Processing & Communication
- Biological & Soft Matter Physics
- Atomic, Molecular & Optical Physics
- Bose–Einstein Condensates & Ultracold Gases
- Metamaterials, Nanostructures & Magnetic Materials
- Mathematical Methods
- Physics of Gases, Plasmas & Electric Fields
- High Energy Nuclear Physics

If you are working on research in any of these areas, the Co-Editors would be delighted to receive your submission. Articles should be submitted via the automated manuscript system at **www.epletters.net**

If you would like further information about our author service or EPL in general, please visit **www.epljournal.org** or e-mail us at **info@epljournal.org**

EPS Società Italiana di Fisica EDP SCIENCES **IOP** Publishing

Image: Ornamental multiplication of space-time figures of temperature transformation rules (adapted from T. S. Bíró and P. Ván 2010 *EPL* **89** 30001; artistic impression by Frédérique Swist).

A Letters Journal Exploring the Frontiers of Physics

February 2014

EPL, **105** (2014) 46003
doi: 10.1209/0295-5075/105/46003

www.epljournal.org

Creep dynamics of viscoelastic interfaces

E. A. Jagla

Centro Atómico Bariloche and Instituto Balseiro, Comisión Nacional de Energía Atómica (8400) Bariloche, Argentina

received 31 October 2013; accepted in final form 5 February 2014
published online 25 February 2014

PACS 68.35.Rh – Phase transitions and critical phenomena
PACS 07.05.Tp – Computer modeling and simulation
PACS 62.20.mm – Structural failure of materials: Fracture

Abstract – The movement of a purely elastic interface driven on a disordered energy potential is characterized by a depinning transition: when the pulling force σ is larger than some critical value σ_1 the system is in a flowing regime and moves at a finite velocity. On the other hand, if $\sigma < \sigma_1$ the interface remains pinned and its velocity is zero. We show that in the case of a one-dimensional interface, the inclusion of viscoelastic relaxation produces the appearance of an intervening regime between the pinned and the flowing phases in a well-defined stress interval $\sigma_0 < \sigma < \sigma_1$, in which the interface evolves through a sequence of avalanches that give rise to a creep process. As $\sigma \to \sigma_0^+$ the creep velocity vanishes as a power law. As $\sigma \to \sigma_1^-$ the creep velocity increases as a power law due to the increase of the typical size of the avalanches. The present observations may serve to improve the understanding of fatigue failure mechanisms.

Copyright © EPLA, 2014

Introduction. – An elastic interface driven through a disordered energy landscape is a generic model for many different physical systems, as domain walls in ferromagnetic materials [1–3], wetting fronts on a rough substrate [4,5], seismic fault dynamics [6–8], and crack propagation [9]. Two generic ways of driving the interface are typically considered. When the interface is forced to move at a small, constant average velocity, the dynamical evolution proceeds through abrupt events called avalanches. When the elastic interface is driven at constant external stress instead, the dynamics is characterized by a depinning transition [10]: Below some critical applied stress σ_1 the interface remains pinned, and the configuration is stationary. Above this threshold, the system does not reach an equilibrium configuration, and the dynamics proceeds continuously in time, in a flowing regime with a finite velocity. This velocity critically vanishes as the applied stress is reduced towards σ_1. Within the context of fracture, the depinning transition is seen as the onset of crack propagation at a finite velocity, producing the failure of the material.

The configurations of the system for $\sigma < \sigma_1$ correspond to metastable minima of the total energy. The existence of these static pinned configurations relies on the absence of thermal activation mechanisms. If temperature is different from zero the energy barriers to escape the metastable minima are eventually surmounted, and the system can creep at a finite velocity [11–13]. The velocities generated by the creep process are much smaller than those of the flowing regime, so the value σ_1 still signals the transition between a low velocity creep regime and a large velocity flow regime. In the presence of thermally activated processes, the velocity of the interface strictly vanishes only when $\sigma \to 0$.

Experimentally, the creep regime may cause fatigue failure [9,14][1] and is a concern in the performance of mechanical components. It may induce failure after a prolonged time of service at applied loads well below the nominal fracture strength. This behavior is captured in some phenomenological laws, as for instance the Basquin law [15], that states that the lifetime of a component is proportional to some negative power of the applied load. The phenomenology of static fatigue failure typically involves additional features that are not appropriately captured by the thermal creep mechanism alone. In many cases a *fatigue limit* exists, such that there is no progression of the damage at all if the applied load is below this limit [14]. Theoretical explanations of this fact have relied upon the existence of *healing mechanisms* in

[1]We refer exclusively here to *static* fatigue failure, that occurs due to a long time application of a *constant* load. It must not be confused with *cyclic* fatigue processes, in which the failure occurs due to the interplay of oscillating loads and plastic effects in the material.

the material [16–18], that compete with creep, generating a fatigue limit at a finite applied load.

In this paper we investigate theoretically an alternative mechanism to thermal creep that can produce the slow advance of an interface on a disordered media, then giving insight into the possible mechanisms of fatigue failure under constant applied loads. The model assumes the existence of viscoelastic effects in the material. In this case even if temperature is set to zero, we find that the interface advances at a finite (but small) velocity in a well-defined range of the applied stress σ, namely $\sigma_0 < \sigma < \sigma_1$. Below σ_0 there is no advance at all, then this value represents the *fatigue limit* of the material. The dynamics close to the fatigue limit can be described as a kind of contact process [19]. The advance of the interface in this viscoelastic creep regime occurs through a sequence of avalanches, that become progressively larger as $\sigma \to \sigma_1$, where the creep regime crosses over to the flow regime. This crossover becomes a sharp transition in the limit in which the temporal scale of the viscoelastic relaxation is much larger than the scale in which individual avalanches develop. In this last case the average size of the creep avalanches diverges as $\sigma \to \sigma_1$.

The paper is organized as follows. In the second section we define in detail the viscoelastic model used, and give details of the numerical simulation technique. Results are presented in the third section, whereas discussions and conclusions are contained in the last section.

Model and simulation technique. – As it was already indicated, the growing of a crack on a material under load, can be described by treating the one dimensional crack front as an elastic interface that is driven through a disordered pinning potential, representing the material imperfections at a microscopic scale (see the discussion around fig. 34 in [9]). An appropriate model that captures the essence of this phenomenon is the one-dimensional quenched Edwards Wilkinson (qEW) model [20] that is schematically represented in fig. 1(a). The equations that govern the evolution of the variables h_i (representing the coordinates of the interface) are

$$\eta \partial_t h_i = F_i + f_i^{dis}(h_i) + k_1 \Delta h_i. \qquad (1)$$

This is an overdamped dynamics for the variables h_i, which are defined on a sequence of discrete sites. Δ indicates the discrete Laplacian, f_i^{dis} (which is negative) represents the pinning forces at different sites, and F_i is the driving force on the interface. Note that the elastic interactions in actual cracks are long ranged. The local form used here (the Laplacian term) is justified on the basis of its simplicity, and must be considered as a first approximatioin to a more realistic modeling.

In *constant force* driving, the value of F_i is constant, and independent of i, and represents the stress applied onto the system, namely $F_i \equiv \sigma$. This is the case in which a critical stress σ_1 exists that separates a pinned regime from a flowing, depinned regime. In *constant velocity* driving F_i is chosen to be of the form $F_i = k_0(Vt - h_i)$, representing a driving at constant velocity V through springs of stiffness k_0. The average stress in the system in this case is given by $\sigma = k_0(Vt - \overline{h_i})$. Constant velocity driving corresponds to the application of a constant strain rate in the fracture context. In the limit of $V \to 0$, the dynamics in the constant velocity case consists of a sequence of avalanches, that have a typical duration that is proportional to η. We will take formally $\eta \to 0$, and in this sense, the avalanches will be considered as instantaneous. Constant velocity driving is connected with constant force driving in the limit $k_0 \to 0$. In fact, in constant velocity driving the values of F_i for all i tend to σ_1 as $k_0 \to 0$ (see below).

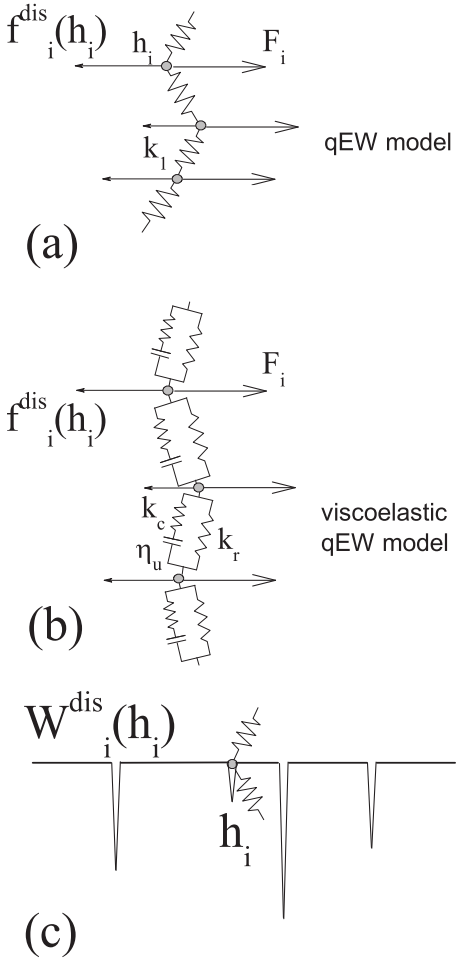

Fig. 1: (a) Sketch of the discrete quenched Edwards-Wilkinson model. (b) The viscoelastic version discussed here. F_i are the driving forces. $F_i \equiv \sigma$ in constant force driving, and $F_i \equiv k_0(Vt - h_i)$ in constant velocity driving. (c) Sketch of one of the sites in the discrete pinning potential used, from which the pinning forces are obtained: $f_i^{dis}(h_i) = -\mathrm{d}W_i^{dis}/\mathrm{d}h_i$. The positions of the narrow pinning wells and their strengths are randomly distributed (see parameters in text).

We work in the case of a discrete pinning potential in which $f_i^{dis}(h_i)$ is different from zero only in some discrete

set of values of h_i, that represent the positions of pinning centers (fig. 1(c)). This is convenient for the numerical implementation, but the results obtained are independent of this choice. Pinning centers are uncorrelated for different positions i. Each pinning center is characterized by the force that is necessary to apply in order to extract a particle from it. These values are noted f_i^{th}, and are drawn from a Gaussian distribution with zero mean and unitary variance. The location of the pinning centers along the h direction is random, with a mean separation $z_0 = 0.1$.

A viscoelastic version of the qEW model was introduced in the constant force set up and studied in mean field approximation by Marchetti *et al.* [21]. Here we use the version presented in [22]. The model takes into account the possibility of relaxation effects in the material, by replacing the k_1 springs by linear viscoelastic elements, as depicted in fig. 1(b). The equations of this model in the constant force setup are given by

$$\eta \partial_t h_i = f_i^{dis}(h_i) + k_r \Delta h_i + D_i + \sigma, \tag{2}$$

where σ is the externally applied constant force, and the additional term D_i represents the forces onto h_i exerted by branches containing the k_c spring. D_i obeys the equation

$$\eta_u \partial_t D_i + k_c D_i = \eta_u k_c (\Delta \partial_t h)_i. \tag{3}$$

Equation (3) describes the relaxation of the force through the k_c branches, due to existence of the dashpot elements, characterized by the viscosity constant η_u. The value of η_u sets a new time scale in the system given by η_u/k_c. We work in the case in which this time scale is much larger than the typical timescale of individual avalanches, namely $\eta_u \gg \eta$. This implies that the solutions to (2), (3) can be obtained through the following protocol. Given some configuration h_i of the interface, D_i relax in time according to

$$D_i(t) = D_i(t_0) \exp\left(-k_c t/\eta_u\right), \tag{4}$$

which is the solution to eq. (2) when h's are kept constant (as it is the case since the pinning centers are discrete). This relaxation is followed until the force onto some h_i reaches its threshold value, namely $D_i + k_r \Delta h_i + \sigma = f_i^{th}$. At this point, an avalanche starts at position i, producing the advance of h_i to the next potential well $h_i \leftarrow h_i + z$ (where z is taken from an exponential distribution with mean $z_0 = 0.1$), and a corresponding rearrangement of D_i according to

$$D_i \leftarrow D_i - 2k_c z, \tag{5}$$

$$D_j \leftarrow D_j + k_c z, \tag{6}$$

where j are the two neighbor sites to i, and the value of f_i^{th} is renewed from its probability distribution. All successive unstable sites are treated in the same way until there are no more unstable sites. Note that due to the time separation condition $\eta_u \gg \eta$ we do not need to care about eq. (4) during the avalanche. Once the avalanche is exhausted, we continue relaxing D_i according to eq. (4) until the next instability.

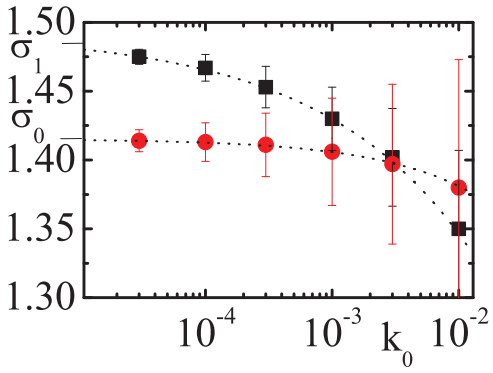

Fig. 2: (Colour on-line) The average stress σ as a function of k_0 in constant velocity driving simulations, for the qEW model (squares, $k_1 = 1$), and the viscoelastic qEW model (circles, $k_r = 0.1$, $k_c = 0.9$) in one dimension. The bars indicate the value of the dispersion of σ, which is observed to tend to zero as $k_0 \to 0$. Dotted lines are power law fittings of the form $\sigma(k_0) = \sigma(0) - \alpha k_0^{\gamma}$. The best fitted values of $\sigma(0)$ in the two cases are $\sigma_0 = 1.415$, and $\sigma_1 = 1.493$.

This scheme is used to study the dynamics of the system for any value of the applied stress σ. All the simulations presented below were made in a system of 2^{14} sites, using periodic boundary conditions. This size is much larger than the largest size of the avalanches observed.

Results. – In [22], the properties of the viscoelastic qEW model were studied both in the mean field limit, and in two spatial dimensions, in the constant velocity driving case. Here we concentrate on the one-dimensional case, that we have found behaves very differently to the higher-dimensional cases discussed in [22] (the reason of this difference is briefly discussed in the conclusions). As a preliminary result, we show in fig. 2 results for the average stress and its fluctuation across the surface in constant (vanishingly small) velocity driving through a spring of value k_0 (see footnote [2]).

Results are shown for a viscoelastic qEW model with $k_r = 0.1$, $k_c = 0.9$, and for a reference qEW model, with $k_1 = k_r + k_c = 1$. We see that in the two cases, the fluctuations of σ across the whole interface (represented as bars in fig. 2) tend to zero as $k_0 \to 0$, indicating a convergence to a constant force driving scenario in both cases in this limit. A fundamental fact of the one-dimensional model is that the limiting value σ_0 for the viscoelastic qEW model is lower than the value σ_1 for the standard qEW model.

On the basis of the these results we will now describe the behavior of the viscoelastic model in the constant force set up. If σ is sufficiently large, there is not any stationary solution to eq. (2). This means that the system evolves by a single avalanche that lasts forever. The dynamics of this

[2]The numerical algorithm in this case is a slight generalization of the one presented in the previous section. Details can be seen in [22].

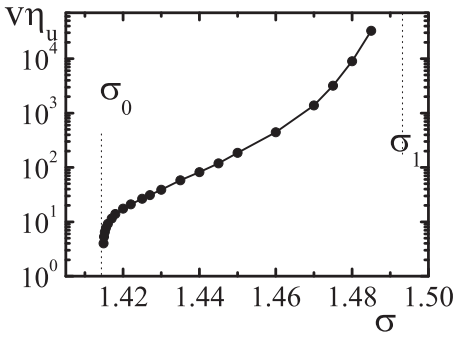

Fig. 3: Velocity as a function of stress in the creep regime. The vertical dotted lines indicate the values of σ_0 and σ_1 from the fits in the previous figure.

avalanche develops in a time scale of the order of η. In our time units in which $\eta \to 0$, we will consider this velocity as diverging, $v \to \infty$. As this dynamics is much more rapid than the viscoelastic one, the dashpots remain blocked during the evolution. This means that in this regime the model behaves as a standard qEW model with an effective elastic constant k_1 of value $k_1 = k_r + k_c$. The value σ_1 in fig. 2 is precisely the depinning stress of this elastic model, so this regime occurs for all $\sigma > \sigma_1$. In the opposite limit of small σ, namely $\sigma < \sigma_0$, the interface reaches a stationary configuration in which it remains pinned, and its velocity is zero.

The intermediate regime $\sigma_0 < \sigma < \sigma_1$ is the viscoelastic creep regime in which we are mostly interested here. We present in fig. 3 the results of numerical simulations in which a constant σ is applied, and the average velocity of the interface is measured. The vanishing of the velocity as $\sigma \to \sigma_0$ is clearly observed in this plot. In the range $\sigma_0 < \sigma < \sigma_1$ the velocity of the interface remains finite (and proportional to η_u^{-1}), indicating that the interface does not reach any globally stable configuration. As $\sigma \to \sigma_1$ we observe a divergence in the velocity. This divergence actually signals the transition from a velocity that is order η_u^{-1} for $\sigma < \sigma_1$, to one of the order of η^{-1} for $\sigma > \sigma_1$. We are interested in characterizing in more detail this intermediate creep regime of the dynamics.

The advance of the interface for $\sigma_0 < \sigma < \sigma_1$ occurs through abrupt avalanches, that are instantaneous for our choice $\eta \to 0$. During avalanches the stretching of the dashpots remain fixed. Immediately after an avalanche, the dashpots are unrelaxed, an tend to equilibrium in a time scale of the order of η_u^{-1}. This relaxation triggers eventually new avalanches that maintain the interface in motion forever. This is the mechanism that generates a velocity of the order of η_u, in the creep regime $\sigma_0 < \sigma < \sigma_1$.

Each avalanche can be characterized by the spatial coordinate i at which it starts, its time of occurrence t and its size S, that is defined as the sum of the displacements of all sites that participate in it. An important quantity to consider is the size distribution of avalanches $N(S)$, such that $N(S)\mathrm{d}S$ is the number of avalanches in the interval

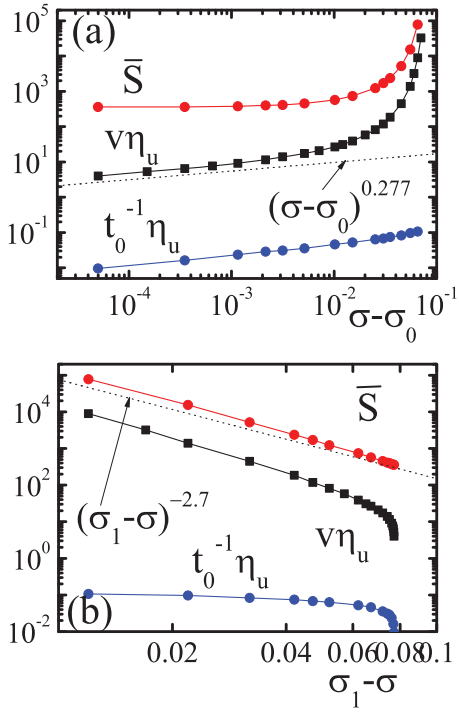

Fig. 4: (Colour on-line) Velocity (squares) as a function of stress and its decomposition as the ratio of an average avalanche size $\overline{S}$ and an inter-avalanche time t_0. The two plots highlight the power law dependencies for $\sigma \to \sigma_0$(a) and $\sigma \to \sigma_1$(b). In (a) the expected result of the velocity as $\sigma \to \sigma_0$ for a directed percolation process is indicated by the dashed line. In (b), the dashed line shows the expected behavior of $\overline{S}$ as $\sigma \to \sigma_1$ from the results of a qEW model with $k_1 = k_r + k_c = 1$. The values of σ_0 and σ_1 here are those obtained from fig. 2.

$[S, S + \mathrm{d}S]$ per unit of time and unit of length in the system. The velocity of the interface can be written in terms of $N(S)$ as

$$v = \int SN(S)\mathrm{d}S. \tag{7}$$

It is convenient to introduce an average time t_0 between avalanches (per unit of system length), such that $t_0 = (\int N(S)\mathrm{d}S)^{-1}$. We can then write v as $v = \overline{S}/t_0$ where $\overline{S} \equiv \int SN(S)\mathrm{d}S / \int N(S)\mathrm{d}S$ is the average size of avalanches. In fig. 4 we plot the results for t_0 and $\overline{S}$ from the numerical simulations. As we see, a divergence of $\overline{S}$ controls the divergence of velocity for $\sigma \to \sigma_1$, whereas a divergence of t_0 controls the vanishing of v for $\sigma \to \sigma_0$.

The size distribution of avalanches for different values of σ is presented in fig. 5. We observe the development of a critical distribution as $\sigma \to \sigma_1$, with a decaying exponent $\tau \simeq 1.11$, which is similar to that corresponding to the qEW model. The scaling of the curves as $\sigma \to \sigma_1$ is rather well described by the qEW values also (fig. 5, inset). An examination of the epicenters of the avalanches in the present case, reveals that they are not temporally nor spatially correlated. This seems reasonable in this regime: if one large avalanche is triggered, relaxation may produce

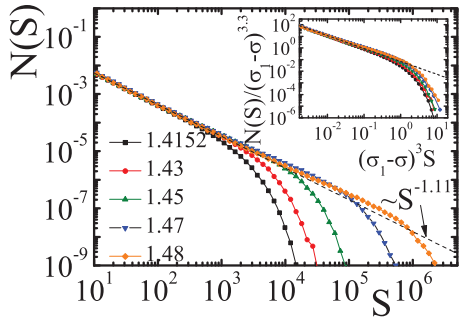

Fig. 5: (Colour on-line) The size distribution of avalanches in the creep regime, for different values of σ, as indicated. The inset shows the scaling of the curves using the known exponents of the qEW model.

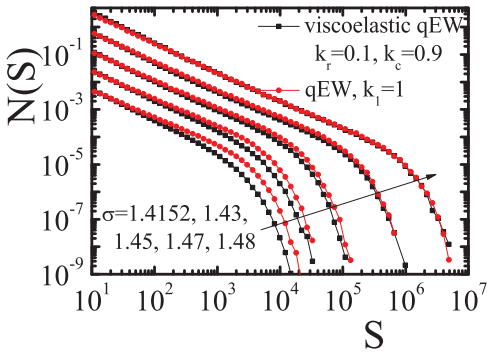

Fig. 6: (Colour on-line) Size distribution of avalanches in the viscoelastic qEW model in the creep regime, compared with the distribution of avalanches in the standard qEW model driven at constant force, in which the avalanches are randomly triggered (pairs of curves at different σ have been vertically displaced for clarity). The distributions in the two cases tend to coincide as $\sigma \to \sigma_1 \simeq 1.493$.

a subsequent avalanche essentially in any point affected by the first one, not necessarily close to the epicenter of the first one. This makes plausible that the size distribution obtained coincides with that of the normal qEW model: the avalanches in the limit $\sigma \to \sigma_1$ are equivalent to those of a normal qEW model with constant force driving, in the case in which avalanches are triggered in random positions of the system. In fact, a direct comparison of the two cases (fig. 6) confirms this equivalence.

Exploiting this equivalence, we can analyze further the results in fig. 4(b). For the qEW model, the divergence of $\overline{S}$ as $\sigma \to \sigma_1$ is given by (see the standard definitions of the exponents in [23]) $\overline{S} \sim S_{max}^{2-\tau} \sim (\sigma_1 - \sigma)^{\nu(2-\tau)(1+\zeta)}$. Using the known values of the exponents for the qEW model we obtain $\overline{S} \sim (\sigma_1 - \sigma)^{2.7}$. This dependence of $\overline{S}$ on $\sigma \to \sigma_1$ controls the divergence of v, as the time between avalanches t_0 becomes constant in this limit. In fig. 4(b) we can see in fact that the behavior of the creep velocity is compatible with this analysis.

When σ is reduced towards σ_0, the mean size of avalanches remains finite, as fig. 4(a) shows. This implies

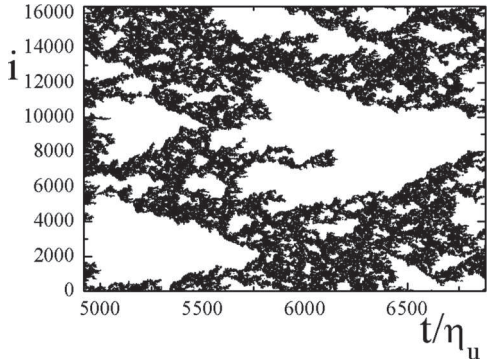

Fig. 7: Epicenters of the events across the system as a function of time, for $\sigma = 1.4152$. The characteristics of a contact process, in which new events are activated by previous nearby ones, is apparent.

that spatial correlations between consecutive avalanches must be observed, as the relaxation of the dashpots can only trigger new avalanches in the close vicinity of regions affected by a previous one. In addition, the vanishing of the creep velocity as $\sigma \to \sigma_0$ implies a divergence of the average inter-avalanche time t_0. It is interesting to look at the spatial distribution of avalanches to see how this happens. We thus run a simulation for σ close to σ_0, and once a stationary creep situation is achieved, plot the location of the epicenters of every event in the system, as a function of time. The result, presented in fig. 7, reveals a striking spatial structure. Those parts of the system that are active at some particular time, continue to trigger avalanches in neighboring places, at a non-singular rate. There are also large spatial and temporal regions that are free of avalanches. As σ is reduced, it is observed that the parts of the system that remain active are more sparse, making the average inter-avalanche time increase.

These findings clarify the way in which creep velocity vanishes as σ_0 is approached. The structure in fig. 7 reveals the existence of a *contact process* [19], in which a given avalanche can activate posterior ones within a time interval of the order of η_u, and no further away than the maximum extension of avalanches (which is limited to about 200 lattice sites for the parameters used here). Although we do not have any other strong evidence, we want to stress the visual similarity of the spatial structure of the epicenter's location in fig. 7 and the structure of a directed percolation process in the active phase (see [19]). If the limit $\sigma \to \sigma_0$ is in fact in the directed percolation universality class, the velocity of the interface (which is proportional to the density of events in fig. 7) must follow a law $v \sim (\sigma - \sigma_0)^\beta$, with $\beta \simeq 0.277$. Our results are not inconsistent with this dependence (see fig. 4(a)), but further analysis is necessary to put it on more solid grounds.

Discussion and conclusions. – In this paper we have analyzed the possibility to describe a fatigue crack

growth situation at constant applied load by modeling the advance of the crack edge through a viscoelastic qEW model. In the absence of any thermally activated effects, we have seen that three clearly separated regimes appear as a function of the applied load: no crack advance if $\sigma < \sigma_0$, unstable crack advance (that describes rapid breaking of the system) if $\sigma > \sigma_1$, and a creep regime if $\sigma_0 < \sigma < \sigma_1$, where the crack velocity is controlled by a viscosity coefficient η_u.

We have analyzed in detail the dynamics of the model in the creep regime. Our model displays naturally a fatigue limit σ_0 below which the advance of the crack is completely halted. As the stress is diminished towards the fatigue limit σ_0, the velocity vanishes as a power law. We have interpreted this behavior in terms of a contact process in which one avalanche can give rise to successive ones within a limited spatial range, and in a typical time controlled by η_u. As $\sigma \to \sigma_1$ the velocity diverges (in the scale of η_u) as a power law, until the unstable crack growth regime sets in for $\sigma > \sigma_1$.

The results presented were obtained for the case of a one-dimensional interface. Although this is the situation of interest to model the crack growth within a solid, it is interesting to ask why the two- or larger-dimensional model does not display the same behavior. The immediate answer is that the curves equivalent to those in fig. 2 show that $\sigma_0 > \sigma_1$ in higher dimensions, thus the regime $\sigma_0 < \sigma < \sigma_1$ simply does not exist. The reason of this difference, that will be elaborated elsewhere, is qualitatively the following. Relaxation can be seen as the adjustment of the rest lenght of the spring that are in series with the dashpots. In two dimensions or higher, this adjustment generates a configuration of the system that is more strongly pinned than in the absence of relaxation, thus making the value of σ_0 larger than σ_1. In one dimension instead, the change of rest lenght of the springs does not produce a more strongly pinned configuration. In the end, this implies that σ_1 is larger than σ_0 in one dimension.

Compared with the thermal creep case [13], the most striking difference of the model studied here is the existence of a fatigue limit, corresponding to a stress below which the time to failure of the system is truly infinite. This behavior, which has been observed experimentally in different materials [14] has been explained before relying in *ad hoc* healing mechanisms [16–18]. Our model provides an alternative possible explanation for this phenomenon that appears exclusively because of the microscopic dynamics of the model. The presented mechanism of viscoelastic creep may thus serve to improve our understanding of failure mechanisms of solids under constant stress.

* * *

This research was financially supported by Consejo Nacional de Investigaciones Científicas y Técnicas (CONICET), Argentina. Partial support from grants PIP/112-2009-0100051 (CONICET, Argentina), and PICT-2012-3032 (ANPCyT, Argentina) is also acknowledged.

REFERENCES

[1] Colaiori F., *Adv. Phys.*, **57** (2008) 287.
[2] Zapperi S., Cizeau P., Durin G. and Stanley H. E., *Phys. Rev. B*, **58** (1998) 6353.
[3] Lemerle S., Ferré J., Chappert C., Mathet V., Giamarchi T. and Le Doussal P., *Phys. Rev. Lett.*, **80** (1998) 849.
[4] Rolley E., Guthmann C., Gombrowicz R. and Repain V., *Phys. Rev. Lett.*, **80** (1998) 2865.
[5] Le Doussal P., Wiese K. J., Moulinet S. and Rolley E., *EPL*, **87** (2009) 56001.
[6] Ben-Zion Y. and Rice J. R., *J. Geophys. Res.*, **98** (1993) 14109.
[7] Fisher D. S., Dahmen K., Ramanathan S. and Ben-Zion Y., *Phys. Rev. Lett.*, **78** (1997) 4885.
[8] Fisher D. S., *Phys. Rep.*, **301** (1998) 113.
[9] Alava M., Nukala P. K. and Zapperi S., *Adv. Phys.*, **55** (2006) 349.
[10] Fisher D. S., *Phys. Rev. B*, **31** (1985) 1396.
[11] Nattermann T. and Scheidl S., *Adv. Phys.*, **49** (2000) 607.
[12] Chauve P., Giamarchi T. and Le Doussal P., *Phys. Rev. B*, **62** (2000) 6241.
[13] Bustingorry S., Kolton A. B. and Giamarchi T., *Phys. Rev. E*, **85** (2012) 021144.
[14] Suresh S., *Fatigue of Materials* (Cambridge University Press, Cambridge, UK) 1998.
[15] Basquin O. H., *Proc. Am. Soc. Testing Mater. ASTEA*, **10** (1910) 625.
[16] Kun F., Carmona H. A., Andrade J. S. jr. and Herrmann H. J., *Phys. Rev. Lett.*, **100** (2008) 094301.
[17] Kun F., Costa M. H., Costa Filho R. N., Andrade J. S. jr., Soares J. B., Zapperi S. and Herrmann H. J., *J. Stat. Mech.* (2007) P02003.
[18] Alava M. J., *J. Stat. Mech.* (2007) N04001.
[19] Hinrichsen H., *Adv. Phys.*, **49** (2000) 815.
[20] Barabasi A. L. and Stanley H. E., *Fractal Concepts in Surface Growth* (Cambridge University Press, Cambridge) 1995.
[21] Marchetti M. C., Middleton A. A. and Prellberg T., *Phys. Rev. Lett.*, **85** (2000) 1104.
[22] Jagla E. A., Landes F. P. and Rosso A., arXiv:1310.5051.
[23] Narayan O. and Fisher D. S., *Phys. Rev. B*, **48** (1993) 7030.